CHARACTERISATION, ANALYSIS AND COMPARISON OF MULTIPLE BIOMASS FUELS USED IN CO-FIRING TRIALS.

V.F. Lay[1,2], C.A. Kirk[1], R.L. Higginson[2], S.C. Hogg[2], C. Davis[3]
[1] Department of Chemistry, [2]Department of Materials, [3] E.On Technology (Ratcliffe) Ltd.
[1,2]Loughborough University, Loughborough, Leicestershire, LE11 3TU.
[3]Technology Centre, Ratcliffe-on-Soar, Nottingham, NG11 0EE.

ABSTRACT: The co-firing of biomass and coal is one method proposed for the reduction of CO_2 emissions. This paper compares synthetic laboratory ash of hemp, coal and eucalyptus and their co-ashed blends with deposits formed during the co-combustion of hemp and coal and eucalyptus and coal. Results show that whilst the results are not in complete agreement a trend towards the formation of Ca-silicates, Ca-Mg silicates and K-Al-Silicates at high temperatures is present in both laboratory ashed samples. The morphology of the particles formed through the different methods differs with larger spherical agglomerates present in the deposits.
Keywords: Ashes, Biomass, Co-Firing, Eucalyptus, Hemp,

1 INTRODUCTION

Environmental concerns arising from the frequent and widespread use of fossil fuels for energy generation have led to greater interest in the use of both dedicated biomass firing and biomass/coal co-firing [1]. The combustion of biomass is widely considered to be carbon neutral as the CO_2 absorbed in photosynthesis during plant growth is then released through combustion [2,3]. It is worth noting, that small amounts of greenhouse gases are emitted during fuel transport and processing. Therefore, to ensure that the process is as carbon neutral as possible, it is desirable that biomass is sourced locally [4]. Increases in biomass usage requires a deeper understanding of the fuels used including combustion properties, fuel characteristics (e.g: calorific value, ash composition, heavy metals present) and ash behaviour (formation of corrosion products or high melting point silicates) [5]. This important analysis should be undertaken prior to full application of the fuels [1]. A review of the behavior of a wide range of biomass during combustion has been undertaken [6,7]. Investigations into the composition of ash produced from biomass firing/co-firing have been carried out alongside the possible applications or uses of the ash including fly ash as components in concrete and for use in road surfaces [1].

Phase transformations, alongside chemical interactions during combustion and pyrolysis, have previously been identified as key questions in relation to biomass firing [6]. Multiple studies into biomass combustion and the transformation behavior of the major inorganic elements contained in the ash have been conducted on a variety of fuels [8–12]. Lindberg *et al.* noted that as some systems may have in excess of 20 elements present in the fuels predicting interactions and deposition will not be straight forward [13].

A study into the composition of several species of woody biomass and types of plant tissue of trees (e.g. needles, bark, stem, shoots) concluded that, due to the inhomogeneous nature of the biomass and variations in plant tissue, producing a representative composition of the whole tree is challenging [14]. Further work modelling the ashing characteristics of five types of plant tissue and comparing against laboratory ashed samples, found the theoretical results to be in good agreement with the samples [15]. The elemental composition of biomasses were found to vary between plant species and genus [16,17]. These studies also showed that the ash composition is likely to vary due to different mineral pathways in the plant itself, as well as sometimes being affected by differing soil characteristics.

Databases such as the BIOBIB database [18] provide useful information on fuels already analysed however, the varying nature of biomasses even between crop and harvest [19,20], may mean that the information cannot be relied upon for 100% accurate information on fuels selected for use in power plants and further analysis may be required. It was found that some entries in the database were missing >20% of values required for peer data comparison (e.g. proximal analysis (C,H,S,N,Cl), ultimate analysis (inorganic ash matrix), calorific value, ash thermal behaviour and heavy metal content) [17].

This paper is to examine the ashing characteristics of three biomasses and one coal as well as two blends (hemp-coal and eucalyptus coal) to examine interactions of phases present in the ash at various temperatures on heating. Data obtained from lab studies are compared to deposits formed during large scale co-firing trials in a $1MW_{th}$ combustion rig.

2 EXPERIMENTAL

Hemp, eucalyptus, Russian coal and two biomass-coal blends, hemp and coal (77:23 by mass) and eucalyptus and coal (88:12 by mass), were ashed in an air atmosphere, in a Carbolite CSF12/13 chamber furnace with a Eurotherm 808 controller. 1g of each sample was ashed in a clean oven dried crucible according to the temperature profile: 150°C (1 hour), 250°C (2 hours), 450°C (1h 30 mins), 575°C (3 hours) followed by cooling in a dessicator, weighing and returning to the furnace at 575°C until a constant weight (±3mg) was obtained. This was carried out in triplicate.

These ashes and ash blends were placed in a Pt crucible in an Elite BRF14/5-2416 Furnace, and heated at 100°C intervals for 1 hour between 600-1100°C. At each temperature, a small portion of each sample was removed and the ash was returned to the furnace.

Fuel analysis was provided by E.On Technology (Ratcliffe) Limited. As received data are presented in **Table I.**

Ash analysis of the bulk fuels was provided by E.On Technology (Ratcliffe) Limited. Elements present were determined by acid dissolution and emission spectroscopy according to ASTM D6349-09. (**Table II**) gives ash analysis.

Table I: Fuel composition, as received provided by E.On Technology (Ratcliffe) Limited

	Hemp	Eucalyptus	Coal
Moisture (%)	14.5	8.2	7.3
Volatile Matter (%)	56.3	76.8	35.8
Fixed Carbon (%)	13.00	14.40	48.20
Ash (%)	16.2	0.6	8.7
CV, kJ/kg	14050	18570	27440
Sulfur (%)	0.09	0.01	0.34
Chlorine (%)	0.21	0.03	0.01
Hydrogen (%)	4.43	5.63	4.48

Table II: Elements present in the ashes of fuels studies as determined by emission spectroscopy, provided by E.On Technology (Ratcliffe) Limited. (CaO as $CaCO_3$ for biomass)

Element (%)	Hemp	Eucalyptus	Coal
SiO_2	44.00	26.50	44.80
Al_2O_3	1.68	7.60	6.21
Fe_2O_3	0.84	5.13	4.50
CaO	17.70	21.80	23.10
MgO	3.89	5.88	2.55
K_2O	11.80	10.25	3.57
Na_2O	0.32	2.52	1.52
TiO_2	0.11	0.33	4.07
BaO	0.02	0.22	0.49
Mn_3O_4	0.17	2.03	0.57
P_2O_5	6.52	2.88	1.13
SO_3	1.44	2.53	3.53

Samples were collected onto ceramic probes (**Figure 1)** in the superheater region of a $1MW_{th}$ test combustion rig. They were taken *in-situ* during combustion runs of the co-firing of hemp-coal (77:23% by mass) and eucalyptus-coal (88:12% by mass). The collection times and temperatures are shown in **Table III**.

Figure 1: Hemp and coal ash deposits onto ceramic probes

Table III: Sample collection parameters for combustion rig samples (H=Hemp, E=Eucalyptus)

Sample	Duration (min)	Temperature (°C)
H1	38	971
H2	57	Not Recorded
H3	76	1013
H4	58	980
E1	163	978
E2	202	914
E3	184	1012
E4	117	932

Samples were prepared for Scanning Electron Microscopy (SEM)- Energy Dispersive X-Ray Spectroscopy (EDS) by placing the ash materials onto a carbon sticky pad attached to an aluminium stub followed by Au coating for 30s. Analysis was carried out using a Leo-Zeiss 1530VP field emission gun (FEG) with an X-Max $80mm^2$ detector (20kV, 60µm aperture, backscatter detector, 8.5mm working distance) or (10kV, 30 µm aperture, SE2 detector (deposit samples)).

Samples were prepared for Powder X-Ray Diffraction (PXRD) by grinding in a pestle and mortar with acetone to a suspension and mounting on a silicon substrate. Powder XRD data were collected using the Bruker D2 PHASER diffractometer (5-60º 2θ, CuKα radiation, 15min, step size 0.0122, 4509 steps, 0.2s time step, 1-Dimentional LYNXEYE detector). Data was analysed using STOE WinXPow software suite and the ICDD 2005 database.

3 RESULTS AND DISCUSSION

Table I illustrates that the fuel compositions differ from one another, with coal and hemp containing a larger portion of ash in comparison to eucalyptus. This, in turn, is likely to have an effect on the slagging and fouling prospensity of a fuel. Larger quantities of ash lead to an increase in the likelihood of phases which can cause the well documented issues [4,21] of high deposition rate and corrosion to occur.

Table II gives the elemental composition of the ash matrices of the three fuels studied. Differences in the quantity of elements present can lead to a significant phase variation between fuels. A comparison of the phases present in laboratory ashed samples to those present in ash samples collected in the combustion rig, may show some differences. This is likely to be due to the reduction/oxidation conditions and atmosphere experienced in each environment differing, which may result in the formation of different phases.

3.1 Laboratory Ashed Samples

3.1.1 X-Ray Diffraction

PXRD data are presented in **Figures 2-4**, representing analysis of samples at 600°C, 1000°C and 1100°C . These temperatures and data sets were selected as they highlight clear differences in the phases present at different temperatures on heating. The PXRD patterns shown in **Figure 2**, show that the major component of the ash at 600°C is quartz (SiO_2). This is unsurprising due to the large percentage of Si present in each of the fuels (**Table I**). At lower temperatures SiO_2 remains largely unreacted. The role of silicates in plants is known to be largely a protection mechanism from stress [22]; it is commonly taken up as sililic acid ($Si(OH)_4$) before transport to other regions of the plant.

At lower temperatures carbonates (calcite ($CaCO_3$), fairchildite ($K_2Ca(CO_3)_2$) and dolomite ($CaMg(CO_3)_2$)) are present. The origin of calcite in the biomass fuels is thought to be via the decomposition of calcium oxalate, known to be present in the fuels [23,24]. The decomposition occurs in two steps:

$CaC_2O_4.H_2O \rightarrow CaC_2O_4 + H_2O$ 170-200°C
(Equation 1) [6]

$CaC_2O_4 \rightarrow CaCO_3 + CO_2$ 300-600°C
(Equation 2) [6]

Calcite often then undergoes a decomposition to lime (CaO) according to the reaction:

$CaCO_3 \rightarrow CaO + CO_2$ 840°C
(**Equation 3**)
Dolomite decomposition follows the path shown in **Equation 4**[25]**.**

$CaMg(CO_3)_2 \rightarrow CaCO_3 + MgO + CO_2$ 500-900℃
(Equation 4)[6]

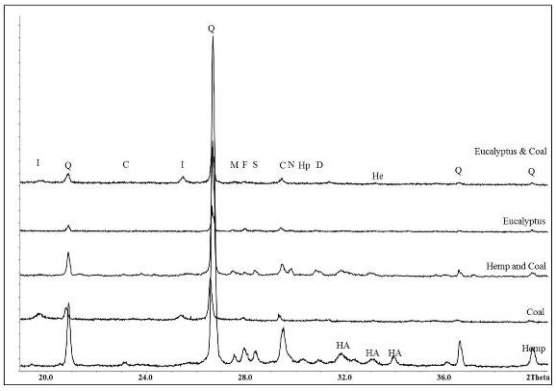

Figure 2: PXRD data of laboratory ashed samples at 600°C. A selected range (20-40°2θ) is presented for clarity. Q (Quartz, SiO_2), M (Microcline, $KAlSi_3O_8$), F (Fairchildite, K_2CaCO_3), S (Sylvite, KCl), C (Calcite, $CaCO_3$), N (Nepheline, $NaAlSiO_4$), Hp (Halite Potassian ($K_{0.4}Na_{0.6}Cl$), D (Dolomite, $CaMg(CO_3)_2$), I (Illite, $K(Al_4Si_2O_9(OH)_3$), HA (hydroxyapatite ($Ca_{9.04}(PO_4)_6(OH)_{1.68}$), He (Hematite, Fe_2O_3). The highest intensity reflection of Periclase (MgO) is observed at 42.9°2θ, outside the range presented. **Tables V-IX** in the appendix list the full phases present in each fuel at each temperature.

The presence of lime was only observed in the sample set for hemp suggesting that upon formation it promptly reacts, most likely to form Ca-silicates.

Above 900°C silicates begin to form (**Figures 3 & 4**). Due to the differing original compositions of the fuels there are a variety of silicates formed for each fuel. All three fuels are high in Ca and therefore the presence of Ca-silicates through the pathways presented in equations 5-7 is likely.

$CaCO_3 + SiO_2 \rightarrow CaSiO_3$ (wollastonite) $+CO_2 + 2CO_2$
(**Equation 5)**[25]

$CaMg(CO_3)_2 + SiO_2 \rightarrow CaMgSi_2O_6$ (diopside) $+ 2CO_2$
(**Equation 6)**[25]

$KAl_2(Si_3Al)O_{10}(OH)_2$ (illite) $+ 2\ CaCO_3 + 4SiO_2 \rightarrow$ $2KAlSi_3O_8$ (leucite) $+ 2Ca_2Al_2SiO_8$ (anorthite) $+ 2CO_2 + H_2O$
(Equation 7)[26]

The formation of the Ca-silicates alongside CaMg-silicates highlights the potential for interaction between the elements and phases present in biomass and coal. For instance, eucalyptus ashed without coal was found to have more prominent peaks associated with akermanite ($Ca_2MgSi_2O_7$) in comparison to the diffraction signature of the more Mg-rich phase, diopside ($CaMgSi_2O_6$), whereas the eucalyptus-coal blend had a more prominent signature of the diopside phases. This suggests that Ca reacted preferentially over Mg to drive formation as shown by Trindade *et al.*, who found that $CaCO_3$ is consumed more rapidly than MgO in the formation of Ca-Mg silicates [25]. Therefore an increase in MgO content of the ash, derived from the dolomite present in the coal during co-ashing, may drive the reactions further towards diopside rather than akermanite.

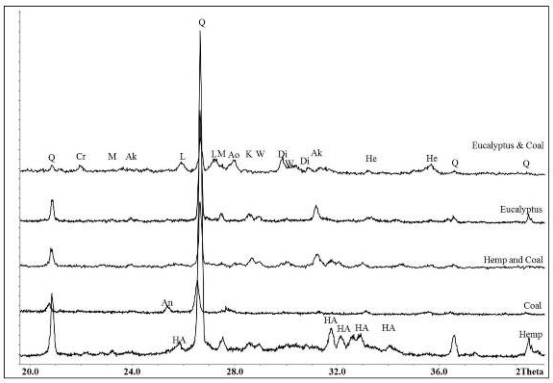

Figure 3: Laboratory ashed samples at 1000°C. A selected range (20-40°2θ) is presented for clarity. Q (Quartz, SiO_2), M (Microcline, $KAlSi_3O_8$), HA (hydroxyapatite ($Ca_{9.04}(PO_4)_6(OH)_{1.68}$), He (Hematite, Fe_2O_3), Di (Diopside, $CaMgSi_2O_6$), K (Kalsilite, $KAlSiO_4$), W (Wollastonite, $CaSiO_3$), Ak (Akermanite, $Ca_2MgSi_2O_7$), L (Leucite, $KAlSi_2O_6$), Ao (Anorthite ($CaAl_2Si_2O_8$), An (Anhydrite ($CaSO_4$)), Cr (Cristobalite, SiO_2). The highest intensity reflection of Periclase (MgO) is observed at 42.9°2θ and Mullite ($Al_{2.35}Si_{0.64}O_{4.82}$), main peak at 16.5°2θ outside the range presented.

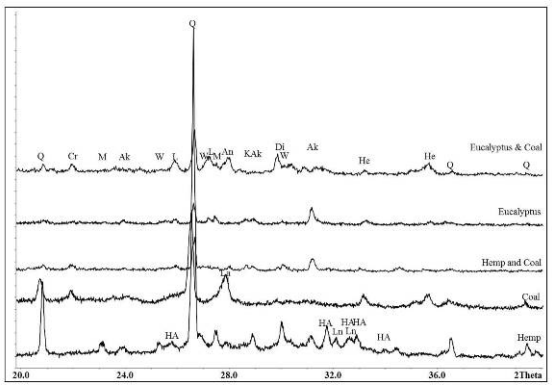

Figure 4: : Laboratory ashed samples at 1100°C. A selected range (20-40°2θ) is presented for clarity. Q (Quartz, SiO_2), M (Microcline, $KAlSi_3O_8$), HA (hydroxyapatite $Ca_{9.04}(PO_4)_6(OH)_{1.68}$), He (Hematite, Fe_2O_3), Di (Diopside, $CaMgSi_2O_6$), K (Kalsilite, $KAlSiO_4$), W (Wollastonite, $CaSiO_3$), Ak (Akermanite, $Ca_2MgSi_2O_7$), L (Leucite, $KAlSi_2O_6$), Ao (Anorthite ($CaAl_2Si_2O_8$), An (Anhydrite $CaSO_4$), Cr (Crisobalite, SiO_2),Ln (Larnite, Ca_2SiO_4). The highest intensity reflection of Periclase (MgO) is observed at 42.923 2θ and Mullite ($Al_{2.35}Si_{0.64}O_{4.82}$), main peak at 16.529 2θ outside the range presented.

Hemp ashed with coal has a greater variety of silicates present in comparison to the ashing of hemp alone (**Tables V & VII**). The lower Fe content of the hemp-coal mixture, in comparison to eucalyptus and coal, for instance may drive the formation of the feldspar anorthite ($CaAl_2Si_2O_8$). Sorenson *et al*. investigated the effects of Fe on the formation of aluminosilicate phases. They concluded that a lower iron content was more likely to yield anorthite rather than diopside, as this mineral was

found to crystallise alongside augite ((Ca,Na)(Mg,Fe,Al,Ti)[(Si,Al)$_2O_6$]) in the presence of Fe [27].

Kang *et al*. classified the effects of Al_2O_3 on the diopside/anorthite system and found that below 8.6wt% Al_2O_3 favoured the formation of diopside over anorthite, Above 15.9wt% Al_2O_3 anorthite was shown to be the dominant phase [28]. The low wt% of Al_2O_3 present in the mixtures suggests a preference towards the formation of diopside. Hemp and coal has a lower Fe content than eucalyptus-coal, favouring anorthite. Increased Al from coal ash in the hemp-coal blend, potentially explains the presence of anorthite in the hemp co-ash where there is none in the hemp ash.

Kalsilite ($KAlSiO_4$) is often present in the ash samples (**Tables V-IX**). Vassilev *et al*., in their comprehensive study of biomass ash transformations state that the formation temperature of kalsilite is between 900-1100°C [6]. This corresponds well with experimental data, however it has been identified in PXRD patterns collected on samples heated below 900°C. The complex nature of the matrix may be a contributing factor in its early formation. Also present in the ash is leucite ($KAlSi_2O_6$), which may have formed from kalsilite. Previous work by Zhang *et al*. has shown kalsilite to be a precursor to leucite formation[29]. Equation 7 shows a pathway for leucite formation through a reaction with illite. Due to the presence of illite in the coal ash it is likely this is mechanism of the leucite formation at lower temperature in the eucalyptus and coal co-ash.

Hematite (Fe_2O_3) is present in the ashes of coal, eucalyptus, coal & eucalyptus and hemp & coal, which is correlated by the iron contents of the fuels (**Table II**).The Fe_2O_3 shown to be present in the hemp & coal ash is highly likely come from the coal. Vassilev *et al.* [6] state that organically bound iron in biomass fuels oxidises to hematite between 200-700°C, this may explain the presence of Fe_2O_3 in the eucalyptus ash, as the eucalyptus fuel was shown to have a high amount of Fe (**Table II**).

Sylvite (KCl) was found to be present in the hemp samples at low temperature. The eucalyptus and coal fuels have low Cl content (**Table I**) and therefore no KCl in the ashes of these fuels was detected by PXRD.

Hydroxyapatite is present in both the hemp ash and the hemp and coal ash; hemp has a relatively high level of P_2O_5 in the ash matrix (**Table II**). The hydroxyapatite could be either extraneous, from the soil or formed as a secondary phase during ashing [22,30]. Boström *et al.* [12] report that the formation of Ca-phosphate phases will occur prior to an Ca/Si interaction.

The origin of the feldspar phase microcline is thought to originate from soil contamination during harvest and processing [12].

3.1.2 Hemp Microscopy Analysis

Figure 5 shows calcium oxalate/carbonate crystals present in the hemp fuel pre-ashing. Exact information on the composition is hard to ascertain due to the high carbonaceous nature of the fuel. In plant material, it is likely the carbonate phase present is CaC_2O_4 and therefore the presence of $CaCO_3$ through the decomposition of oxalate is likely (**Equation 2**).

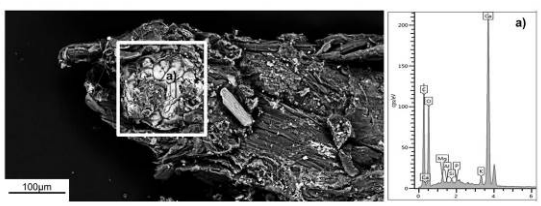

Figure 5: SEM electromicrogaph and EDS analysis of $CaC_2O_4/CaCO_3$ crystals (labelled a) present in hemp fuel.

Figure 6a shows interesting thorn-like structures on the surface of the hemp fuel. Whilst the original texture of the hemp fuel is lost during heating, largely due to its organic composition, these structures remain clearly intact through the heating process. EDS analysis of these structures (**Figure 7**) shows the major components are Ca,K,Mg,Si, P and O, suggesting they comprise of both silicates and hydroxyapatite, this would account for the stability at high temperatures.

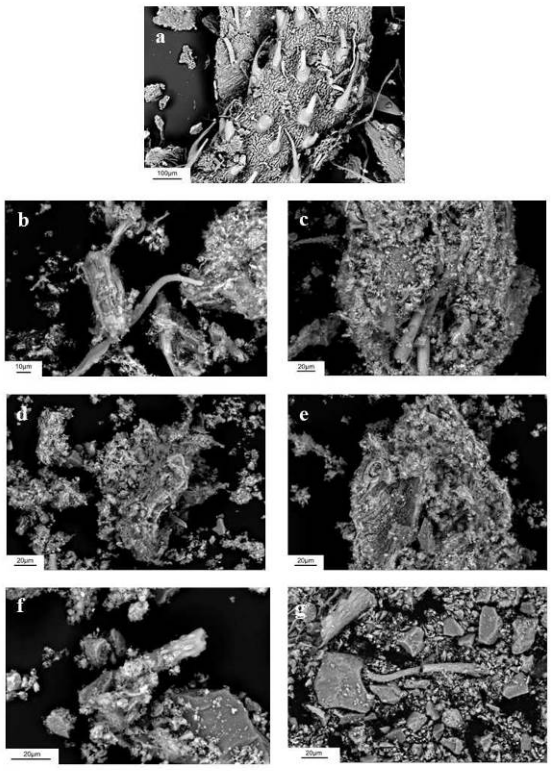

Figure 6: SEM electromicrographs of:- a) hemp fuel b) hemp ash after 1h 600°C
c) hemp ash after 1h 700°C d) hemp ash after 1h 800°C
e) hemp ash after 1h 900°C f) hemp ash after 1h 1000°C
g) hemp ash after 1h 1100°C

As the ashing temperature increased a higher number of glass-like particles are present. This suggests the melting, reaction and agglomeration of certain components of the fuels. EDS mapping (**Figure 8**) shows that these glassy particles largely comprise of Ca-Mg silicates alongside K-Al silicates. Ca and P also remain closely associated. This would confirm the presence of hydroxyapatite, which is thermally stable at 1100°C.

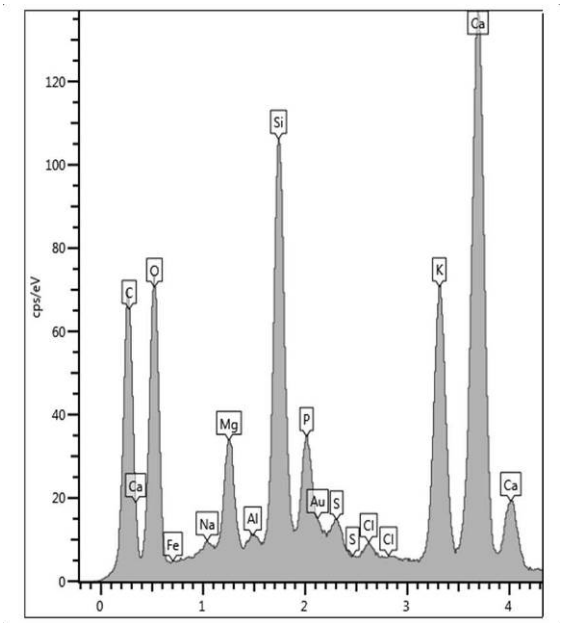

Figure 7: EDS analysis of a thorn-like structure from hemp ash sample at 800°C

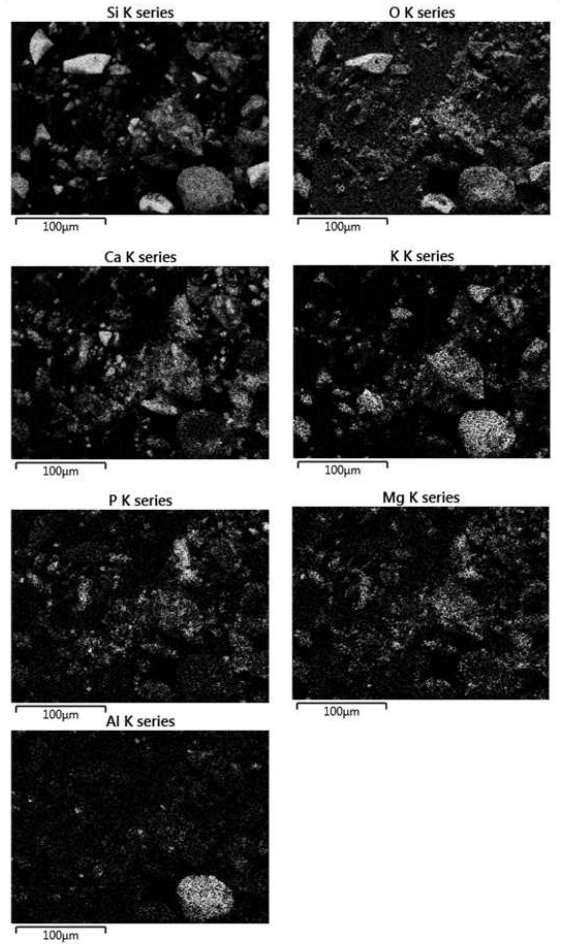

Figure 8: SEM electromicrographs EDS maps of hemp ash at 1100°C

3.1.3 Eucalyptus Microscopy Analysis

An SEM electromicrograph of the eucalyptus fuel (**Figure 9a**) shows a large degree of texture on the fuel surface. This is lost during the ashing process indicating it is cellulose, hemicellulose and lignin that form this structure. After removal of the organic material distinct crystals are observed in the fuels (**Figures 9b-9g**).

EDS analysis shows distinct K,Al,Si,O crystals (**Figure 9b**) at 600°C, thought to be microcline ($KAlSi_3O_8$) as this is the phase containing those elements present at this temperature from XRD (**Table IX**).

Present at 800°C is an anhydrite ($CaSO_4$) crystal probably originating from coal via dehydration of gypsum ($CaSO_4.2H_2O$); this indicates little reaction between certain components of eucalyptus and coal ash until higher temperatures are reached.

The Fe crystals present in **Figure 9e** are thought to originate from fuel processing.

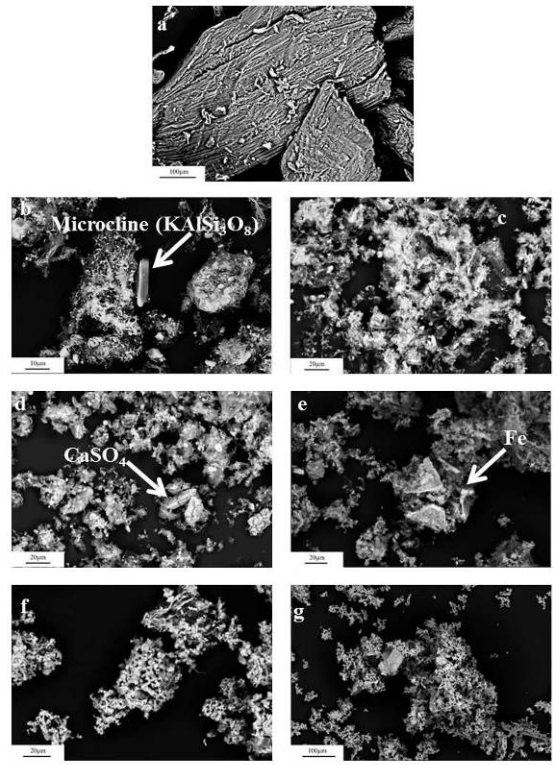

Figure 9: SEM electromicrographs of a) Eucalyptus fuel b) Eucalyptus ash after 1h 600°C c) Eucalyptus ash after 1h 700°C d) Eucalyptus ash after 1h 800°C e) Eucalyptus ash after 1h 900°C
f) Eucalyptus ash after 1h 1000°C g) Eucalyptus ash after 1h 1100°C

3.2 COMBUSTION RIG SAMPLES

To further this investigation, comparison of the data collected on samples from lab-based studies to those collected during combustion rig runs, will now be made. This part of the study focuses on comparisons between the hemp & coal and eucalyptus & coal blends.

3.2.1 P-XRD Analysis

3.2.2 Hemp and Coal Co-Fire

PXRD analysis of the hemp ash samples shows compositional differences between H1-H4 (**Table IV, Figure 10**). The phases found to be present in H2 deviate most when compared to the other samples (H1, H3, H4). Dolomite was shown to be present, with

diopside being the most significant CaMg-silicate phase. In the other samples however, the Ca-Mg silicate akermanite was found to be present. It is also worth noting that the temperature for H2 is unknown and therefore accurate interpretation of the phases present is not fully possible. The presence of dolomite alongside diopside in H2 suggests that there was not a full reaction of dolomite into Ca-Mg silicates and therefore it may have formed from reaction of CaO and MgO with atmospheric CO_2. Vassilev *et al.* show the formation of secondary carbonates between 200-900°C [1].

Variations between samples may also be attributed to temperature differences between samples (971-1013°C) and also reduction/oxidation conditions at the time of sampling [31]. The lack of KCl present in the deposits is due to the temperatures of the ceramic probes; KCl usually deposits through a diffusion/thermophoresis mechanism [32] on to a cool surface. As the temperatures of the ceramic probes used for deposition were at approximately the same temperature as the flue gas it is unlikely that KCl would be present in the samples.

A comparison of the laboratory ashed samples to the combustion rig samples shows many similarities in the phases found to be present. The presence of hydroxyapatite in both sample sets do not indicate whether it is formed during the ashing process or if it is present in the plant itself, possibly in the thorn-like structures. Microcline is only present in some of the rig samples, this suggests that it is extraneous in origin i.e: collected during harvesting from the soil. Extraneous minerals behave differently to those found in the biomass, for instance they may reach lower surface temperatures during combustion [33], or, due to their larger crystallite size (as they will not volatilize in the flame) they may also fail to be carried in the flue gas and drop into the ash hopper, explaining its absence in the rig samples.

The different silicates present in each set of samples can be attributed to the non-equilibrium state of the combustion rig and therefore, whilst the laboratory ashed samples provide some prediction of phases likely to form, in the temperatures of the rig there are some deviations in those found in the rig samples due to the different conditions.

3.2.3 Eucalyptus and Coal Co-Fire P-XRD

Comparison of the PXRD data collected for eucalyptus and coal (**Table V, Figure 11)**to that of the hemp and coal co-fire (**Table IV, Figure 10**) shows the eucalyptus and coal blend deposits to be much more uniform in composition throughout the combustion run. The lower ash content of the eucalyptus in comparison to coal (0.6 and 16.2% respectively) suggests that as there is less variation in the phases capable of forming the ash.
The similarities in phases formed in the eucalyptus co-fire (sample E1-E4) also suggest much more uniform oxidation/reduction conditions. However it should be noted that the sample collection time for eucalyptus was two-three times longer than the hemp samples (**Table III**) suggesting that residence time in the combustion environment plays a key role in reaching conditions where phases become more uniform and stable

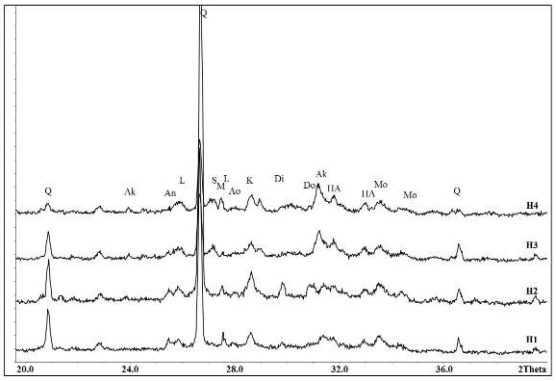

Figure 10: XRD Pattern for combustion rig samples for hemp and coal co-fire. A selected range (20-40°2θ) presented for clarity. Q (Quartz, SiO_2), M (Microcline, $KAlSi_3O_8$), Di (Diopside, $CaMgSi_2O_6$), K (Kalsilite, $KAlSiO_4$), S (Sanidine, $KAlSi_3O_8$), Ak (Akermanite, $Ca_2MgSi_2O_7$), L (Leucite, $KAlSi_2O_6$), HA (hydroxyapatite $Ca_{9.04}(PO_4)_6(OH)_{1.68}$), Mo (monticellite, $CaMgSiO_4$), Ao (Anorthite $CaAl_2Si_2O_8$), An (Anhydrite $CaSO_4$), Do (Dolomite $CaMg(CO_3)_2$) The highest intensity reflection of Periclase (MgO) is observed at 42.923 2θ and Mullite ($Al_{2.35}Si_{0.64}O_{4.82}$), main peak at 16.529 2θ outside the range presented.

Table IV: Phases identified in samples H1-H4 from hemp and coal co-fired combustion run

	H1	**H2**	**H3**	**H4**
Quartz (SiO_2)	•	•	•	•
Akermanite ($Ca_2MgSi_2O_7$)	•		•	•
Diopside ($CaMgSi_2O_6$)	•	•		•
Hematite (Fe_2O_3)			•	•
Anhydrite ($CaSO_4$)	•	•	•	
Leucite ($KAlSi_2O_6$)	•			•
Dolomite ($CaMg(CO_3)_2$)	•	•		
Hydroxylapatite ($Ca_{9.04}(PO_4)_6(OH)_{1.68}$)	•	•	•	•
Forsterite (Mg_2SiO_4)			•	
Monticellite ($CaMgSiO_4$)	•	•	•	•
Kalsilite ($KAlSiO_4$)	•	•	•	
Albite ($NaAlSi_3O_8$)	•			
Periclase (MgO)	•	•	•	•
Microcline ($KAlSi_3O_8$)		•		•
Gehlenite ($Ca_2Al_2SiO_{7)}$		•		
Wollastonite ($CaSiO_3$)			•	•
Sanidine ($KAlSi_3O_8$)			•	•
Mullite ($Al_{2.35}Si_{0.64}O_{4.82}$)			•	•

. Alongside Ca-Mg-silicates, Mg-silicates are also present. As has been previously stated, $CaCO_3$ preferentially reacts with SiO_2 during dolomite decomposition favouring diopside and akermanite formation, the presence of forsterite (Mg_2SiO_4) indicates that a longer residence time may lead to a greater number of chemical reactions in the ash.

Table V: Phases identified in samples E1-E4 from a eucalyptus and coal co-fired combustion run

	E1	E2	E3	E4
Quartz (SiO_2)	•	•	•	•
Akermanite ($Ca_2MgSi_2O_7$)	•	•	•	•
Diopside ($CaMgSi_2O_6$)	•	•	•	•
Hematite(Fe_2O_3)	•	•	•	•
Anhydrite ($CaSO_4$)	•	•	•	•
Leucite ($KAlSi_2O_6$)	•	•	•	•
Dolomite ($CaMg(CO_3)_2$)	•	•	•	•
Aluminium Oxide (Al_2O_3)	•	•	•	•
Forsterite (Mg_2SiO_4)	•	•	•	•
Anorthite ($CaAl_2Si_2O_8$)	•	•	•	•
Rutile (TiO_2)	•	•	•	•
Albite ($NaAlSi_3O_8$)	•	•	•	•

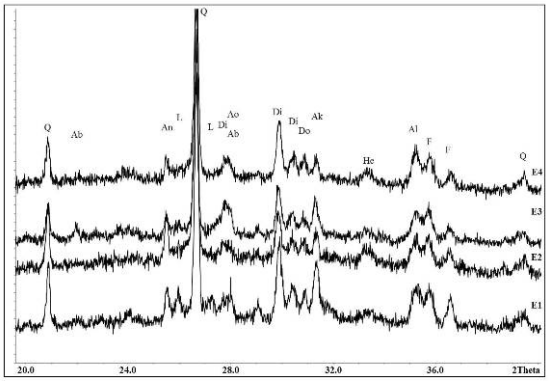

Figure 11: XRD Pattern for combustion rig samples for eucalyptus and coal co-fire. Region 20-40° is presented for clarity. Q (Quartz, SiO_2), Ab (Albite, $NaAlSi_3O_8$), Di (Diopside, $CaMgSi_2O_6$), Ak (Akermanite, $Ca_2MgSi_2O_7$), L (Leucite, $KAlSi_2O_6$), Ao (Anorthite ($CaAl_2Si_2O_8$), An (Anhydrite ($CaSO_4$)) He (Hematite, Fe_2O_3), F (Forsterite, Mg_2SiO_4) Al (aluminium oxide, Al_2O_3)

The lack of kalsilite, but presence of leucite, once again suggests that longer exposure to a high temperature environment has an effect on sample composition. **Equation 7** gives a mechanism of formation for both leucite and anorthite, with the presence of both illite and calcite in the fuel. Future work ashing the eucalyptus and coal under laboratory conditions for longer time periods would be useful for predicting the ash compounds in the combustion rig.

3.2.4 Microscopy of the Co-Fired Rig Samples

Micrographs of the co-fired samples show a distinct spherical morphology for the vast majority of particles in the deposits. The mechanism of deposition for these fly ash particles is inertial impaction, which occurs when large particles (>10μm) have too much mass/inertia to deviate from the gas flow and therefore hit the surface of the tube/deposit[32].

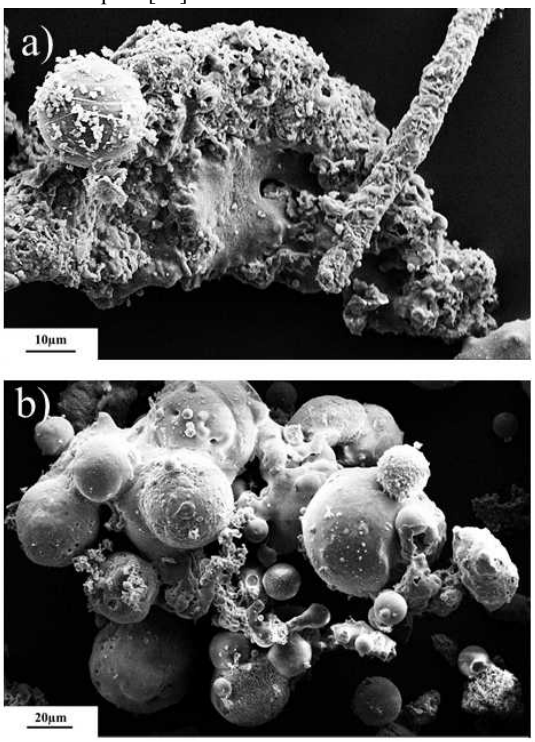

Figure 12: a) SEM electromicrograph of hemp and coal ash deposits removed from a ceramic probe showing particle agglomeration and surface deposition, sample H2. B) SEM electromicrograph of eucalyptus and coal ash deposits removed from a ceramic probe showing a large amount of spherical particles agglomerated together, sample E1.

These deposits form a characteristic elliptical shape as they form on the same side as the gas flow[34], this elliptical shape is shown in **Figure 1**. Inertial impaction in these deposits is also evidenced by the agglomerated particle morphology. Clear fusion between some of the spheres was observed (**Figure 12b**) suggesting reactions may be occurring at these interfaces.

The thorn-like structures which were present in the SEM analysis of hemp and coal (Section 3.1.2), are still observed in deposits from the hemp and coal. **Figure 13** shows EDS analysis of one of these structures which is similar to the analysis presented in **Figure 7**, suggesting the parameters for ash formation have little effect.

The particle surfaces are not always smooth (**Figure 14**) suggesting formation of phases on the surface of the particles. This often occurs through heterogenous nucleation, where refractory oxides (e.g. SiO_2, MgO, CaO etc. or KCl, K_2SO_4 or K_2CO_3) condense with the same species and often form enriched areas on particles surfaces.

In comparison to the morphology of the laboratory ashed samples the spherical particles seen in the rig deposits are much larger. Raask investigated the formation of cenospheres and plerospheres

(aluminosilicate glass microspheres encapsulating gas and smaller pre-existing particles respectively) during coal combustion[35].

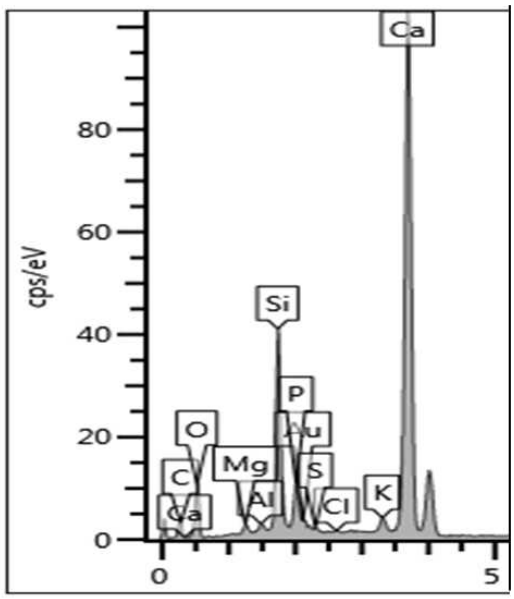

Figure 13: EDS analysis of thorn-like structure from sample H3.

The spheres, which must contain a small amount of Fe and C, form through the expansion of silicate droplets to form a hollow sphere. It is likely that this is a formation mechanism for some of the spheres present in the deposit. These spheres may also form due to the gas conditions present in the combustion rig as one of the main mechanisms in fly ash formation is agglomeration [36].

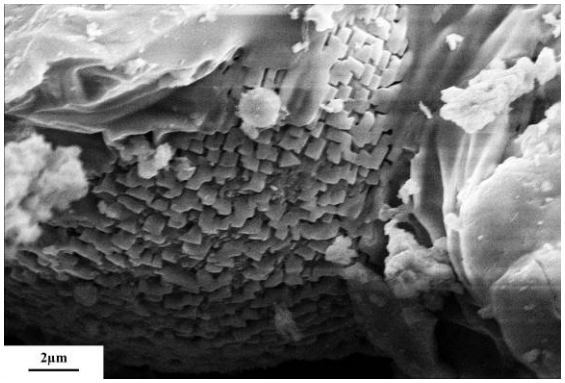

Figure 14: An SEM electromicrograph showing a spherical particle from the hemp and coal co-fire with surface enrichment of cubic crystals.

4 CONCLUSIONS

This paper highlights the benefits from carrying out controlled laboratory ashing studies of fuels to predict fly ash deposition of the same fuels in a combustion rig/power plant. There are many similarities between samples ashed in a controlled environment, at temperatures analogous to those logged during deposition of samples in the combustion rig. The differences between laboratory ashed and combustion rig fired samples indicate that the amount of time a deposit spends in the high temperature environment can have a significant effect on the phases formed.

At high temperatures the main phases, other than quartz identified as present in deposits are Ca-silicates and Ca-Mg-silicates. These are likely to have formed through a reaction between calcite, dolomite, periclase and quartz. The formation conditions of the phases present in ash samples are similar to those conditions used during ceramic phase formation.

SEM studies have shown that the morphology of particles/phases formed during laboratory ashing of the fuels differs to the morphology from those formed under combustion rig conditions. The morphology of particles formed in the rig were more spherical with the spheres present from the combustion rig being larger and are likely formed through a cenosphere/plerosphere mechanism. The conditions required for the formation of these spheres is challenging to replicate under laboratory conditions.

We have shown that controlled laboratory studies produce useful data that can allow predictions of the phase composition of ash deposits in the combustion rig to be made. This could be used alongside modelling to provide a relatively quick, cheap and effective method of assessing a fuel prior to large scale combustion tests.

Future work on the samples includes longer ashing of the coal-biomass blends in the laboratory to determine if the phases formed are similar in composition to those exposed to the high-temperature rig environment for periods longer than 60 minutes. Phase quantification of the PXRD data is also underway to investigate how the proportions of phases alter as a function of temperature.

5 REFERENCES

[1] S.V.Vassilev, D. Baxter, L. K. Andersen, C. G. Vassileva, An overview of the composition and application of biomass ash. Part 1. Phase-mineral and chemical composition and classification, Fuel. 105 (2013) 40-76

[2] K. E. Coleman, N. J. Simms, P. J. Kilgallon, J. E. Oakley, Corrosion in biomass combustion systems, Mater. Sci. Forum. 595-598 (2008) 377-386

[3] S. S. Lokare, J. D. Dunaway, D. Moulton, D. Rogers, D. R. Tree, L. L. Baxter, Investigation of ash deposition rates for a suite of biomass fuels and fuel blends, Energy & Fuels, 20 (2006) 1008-1014

[4] S. Van Loo, J. Koppejan, The handbook of biomass combustion and co-firing, 1st Edition, Earthscan, London, 2008

[5] K. Szemmelveisz, I. Szűcs, Á.B. Palotás, L. Winkler, E.G. Eddings, Examination of the combustion conditions of herbaceous biomass, Fuel Process. Technol. 90 (2009) 839–847.

[6] S. V. Vassilev, D. Baxter, C.G. Vassileva, An overview of the behaviour of biomass during combustion: Part I. Phase-mineral transformations of organic and inorganic matter, Fuel. 112 (2013) 391–449.

[7] S. V. Vassilev, D. Baxter, C.G. Vassileva, An overview of the behaviour of biomass during combustion: Part II. Ash fusion and ash formation mechanisms of biomass types, Fuel. 117 (2014) 152–183.

[8] L.L. Baxter, T.R. Miles, B.M. Jenkins, T. Milne, D. Dayton, R.W. Bryers, et al., The behavior of inorganic material in biomass-fired power boilers :

field and laboratory experiences, Fuel Process. Technol. 54 (1998) 47–78.
[9] S. Miller, B. Miller, The occurrence of inorganic elements in various biofuels and its effect on ash chemistry and behavior and use in combustion products, Fuel Process. Technol. 88 (2007) 1155–1164.
[10] J. Werther, M. Saenger, E.-U. Hartge, T. Ogada, Z. Siagi, Combustion of agricultural residues, Prog. Energy Combust. Sci. 26 (2000) 1–27.
[11] Y. Zheng, P.A. Jensen, A.D. Jensen, B. Sander, H. Junker, Ash transformation during co-firing coal and straw, Fuel. 86 (2007) 1008–1020
[12] D. Boström, M. Broström, Ash transformation chemistry during combustion of biomass, Energy & Fuels 26 (2011) 85-93.
[13] D. Lindberg, R. Backman, P. Chartrand, M. Hupa, Towards a comprehensive thermodynamic database for ash-forming elements in biomass and waste combustion — Current situation and future developments, Fuel Process. Technol. 105 (2013) 129–141.
[14] J. Werkelin, B.-J. Skrifvars, M. Hupa, Ash-forming elements in four Scandinavian wood species. Part 1: Summer harvest, Biomass and Bioenergy. 29 (2005) 451–466.
[15] J. Werkelin, D. Lindberg, D. Boström, B.-J. Skrifvars, M. Hupa, Ash-forming elements in four Scandinavian wood species part 3: Combustion of five spruce samples, Biomass and Bioenergy. 35 (2011) 725–733.
[16] G. Tao, T. a. Lestander, P. Geladi, S. Xiong, Biomass properties in association with plant species and assortments I: A synthesis based on literature data of energy properties, Renew. Sustain. Energy Rev. 16 (2012) 3481–3506
[17] G. Tao, P. Geladi, T. a. Lestander, S. Xiong, Biomass properties in association with plant species and assortments. II: A synthesis based on literature data for ash elements, Renew. Sustain. Energy Rev. 16 (2012) 3507–3522.
[18] H.H. K. Reisinger, C. Haslinger, M. Herger, BIOBIB - A DATABASE FOR BIOFUELS, (n.d.). http://cdmaster2.vt.tuwien.ac.at/biobib/all.html (accessed May 27, 2013).
[19] S. Xiong, Q.-G. Zhang, D.-Y. Zhang, R. Olsson, Influence of harvest time on fuel characteristics of five potential energy crops in northern China., Bioresour. Technol. 99 (2008) 479–85.
[20] T. Prade, M. Finell, S.-E. Svensson, J.E. Mattsson, Effect of harvest date on combustion related fuel properties of industrial hemp (Cannabis sativa L.), Fuel. 102 (2012) 592–604.
[21] R. Frandsen, M. Montgomery, O. H. Larsen, Field test corrosion experiences when co-firing straw and coal: 10 year status within Elsam, Mater. High. Temp. 24 (2007) 343–349.
[22] J.F. Ma, N. Yamaji, Functions and transport of silicon in plants., Cell. Mol. Life Sci. 65 (2008) 3049–57.
[23] M. Etienne, Time factor in utilization of mineral nutrients by hemp, Plant Physiol. (1936) 731.
[24] P. A. Nakata, Advances in our understanding of calcium oxalate crystal formation and function in plants, Plant Sci. 164 (2003) 901–909
[25] M. Trindade, M. Dias, J. Coroado, F. Rocha, Mineralogical transformations of calcareous rich clays with firing: A comparative study between calcite and dolomite rich clays from Algarve, Portugal, Appl. Clay Sci. 42 (2009) 345–355
[26] G. Cultrone, C. Rodriguez-Navarro, E.Sebastian, O. Cazalla, M. J. De La Torre, Carbonate and silicate phase reactions during ceramic firing, Eur. J. Mineral. 13 (2001) 612-634
[27] P.M. Sørensen, M. Pind, Y.Z. Yue, R.D. Rawlings, A. R. Boccaccini, E.R. Nielsen, Effect of the redox state and concentration of iron on the crystallization behavior of iron-rich aluminosilicate glasses, J. Non. Cryst. Solids. 351 (2005) 1246–1253.
[28] M. Kang, S. Kang, Influence of Al2O3 additions on the crystallization mechanism and properties of diopside/anorthite hybrid glass-ceramics for LED packaging materials, J. Cryst. Growth. 326 (2011) 124–127.
[29] Y. Zhang, B. Li, P. Rao, M. Lü, J. Wu, Seeded Crystallization of Leucite, J. Am. Ceram. Soc. 90 (2007) 1615–1618.
[30] S. V. Vassilev, D. Baxter, L.K. Andersen, C.G. Vassileva, T.J. Morgan, An overview of the organic and inorganic phase composition of biomass, Fuel. 94 (2012) 1–33.
[31] P.F.B. Hansen, K.H. Andersen, K. Wieck-Hansen, Co-firing straw and coal in a 150-MW e utility boiler : in situ measurements, Fuel Process. Technol. 54 (1998) 207–225.
[32] A. Zbogar, F. Frandsen, P.A. Jensen, P. Glarborg, Shedding of ash deposits, Prog. Energy Combust. Sci. 35 (2009) 31–56.
[33] M. Cieplik, L. Fryda, Ash Formation, Slagging and Fouling in Biomass Co-firing in Pulverised-fuel Boilers, in: Solid Biofuels for Energy, 2011: pp. 197–217.
[34] L.A. Hansen, H.P. Nielsen, F.J. Frandsen, Influence of deposit formation on corrosion at a straw-fired boiler, Fuel Process. Technol. 64 (2000) 189–209.
[35] E. Raask, Mineral Impurities in Coal Combustion: Behavior, Problems, and Remedial Measures, Taylor & Francis, 1985.
[36] K.A. Christensen, The formation of submicron particles from the combustion of straw, Technical University of Denmark, 1995.

6 ACKNOWLEDGEMENTS

The authors are grateful to the staff at LMCC for the help given during sample analysis. E.On Technology (Ratcliffe) Limited, for providing samples used in the analysis and funding alongside the EPRSC for the provision of funding.

7 APPENDIX

Due to the inhomogenous nature of the samples certain phases are only present in very small amounts and therefore may not always be observed.

Table V: Phases present in laboratory ashed samples of hemp.

Phase	Temperature (°C)					
	600	700	800	900	1000	1100
Quartz (SiO_2)	•	•	•	•	•	•
Calcite ($CaCO_3$)	•	•				
Sylvite (KCl)	•	•	•	•		
Fairchildite ($K_2Ca(CO_3)_2$)	•	•	•			
Hydroxyapatite ($Ca_{9.04}(PO_4)_6(OH)_{1.68}$)	•	•	•	•	•	•
Microcline ($KAlSi_3O_8$)	•	•	•	•	•	•
Periclase (MgO)	•	•	•	•	•	•
Halite, potassian ($K_{0.4}Na_{0.6}Cl$)	•	•	•			
Dolomite ($CaMg(CO_3)_2$	•	•	•			
Lime CaO)			•			
Wollastonite ($CaSiO_3$)			•		•	•
Diopside ($CaMgSi_2O_6$)			•	•	•	•
Akermanite ($Ca_2MgSi_2O_7$)					•	•
Larnite (Ca_2SiO_4)					•	•
Kalsilite ($KAlSiO_4$)					•	

Table VI: Phases present in laboratory ashed samples of coal.

Phase	Temperature (°C)					
	600	700	800	900	1000	1100
Quartz (SiO_2)	•	•	•	•	•	•
Calcite ($CaCO_3$)	•					
Dolomite ($CaMg(CO_3)_2$	•					
Illite ($K(Al_4Si_2O_9(OH)_3$)	•	•	•	•		
Anhydrite ($CaSO_4$)	•	•	•	•	•	
Cuprite (Cu_2O)		•		•	•	•
Hematite (Fe_2O_3)		•	•	•	•	•
Albite ($NaAlSi_3O_8$)					•	•
Labradorite ($Ca_{0.65}Na_{0.32}(Al_{1.62}Si_{2.38}O_8)$						•
Mullite ($Al_{2.35}Si_{0.64}O_{4.82}$)						•

Table VII: Phases present in laboratory ashed samples of hemp and coal

Phase	Temperature (°C)					
	600	700	800	900	1000	1100
Quartz (SiO_2)	•	•	•	•	•	•
Calcite ($CaCO_3$)	•	•	•			
Sylvite (KCl)	•	•	•			
Fairchildite ($K_2Ca(CO_3)_2$)	•	•	•			
Hydroxyapatite ($Ca_{9.04}(PO_4)_6(OH)_{1.68}$)	•	•	•	•	•	•
Microcline ($KAlSi_3O_8$)	•	•	•	•	•	•
Periclase (MgO)	•	•	•	•	•	•
Hematite (Fe_2O_3)	•	•	•	•	•	•
Dolomite ($CaMg(CO_3)_2$	•	•				
Illite ($K(Al_4Si_2O_9(OH)_3$)	•	•				
Nepheline ($NaAlSiO_4$)	•	•	•			
Wollastonite ($CaSiO_3$)				•	•	•
Diopside ($CaMgSi_2O_6$)				•	•	•
Akermanite ($Ca_2MgSi_2O_7$)				•	•	•
Kalsilite ($KAlSiO_4$)				•	•	•
Anorthite ($CaAl_2Si_2O_8$)					•	•
Larnite (Ca_2SiO_4)					•	
Mullite ($Al_{2.35}Si_{0.64}O_{4.82}$)					•	•

Table VIII: Phases present in laboratory ashed samples of eucalyptus

Phase	Temperature (°C)					
	600	700	800	900	1000	1100
Quartz (SiO_2)	•	•	•	•	•	•
Calcite ($CaCO_3$)	•	•				
Fairchildite ($K_2Ca(CO_3)_2$)	•	•				
Microcline ($KAlSi_3O_8$)	•	•		•	•	•
Sylvite (KCl)	•					
Periclase (MgO)			•	•	•	•
Hematite (Fe_2O_3)	•	•	•	•	•	•
Arcanite (K_2SO_4)	•	•	•			
Cristobalite (SiO_2)						•
Wollastonite ($CaSiO_3$)					•	•
Diopside ($CaMgSi_2O_6$)				•		
Akermanite ($Ca_2MgSi_2O_7$)				•	•	•
Leucite ($KAlSi_2O_6$)						•
Kalsilite ($KAlSiO_4$)		•	•	•	•	•
Mullite ($Al_{2.35}Si_{0.64}O_{4.82}$)						•

Table IX: Phases present in laboratory ashed samples of eucalyptus and coal

Phase	Temperature (°C)					
	600	700	800	900	1000	1100
Quartz (SiO_2)	•	•	•	•	•	•
Calcite ($CaCO_3$)	•		•			
Fairchildite ($K_2Ca(CO_3)_2$)	•	•				
Microcline ($KAlSi_3O_8$)	•	•	•	•	•	•
Illite ($K(Al_4Si_2O_9(OH)_3)$)	•	•				
Periclase (MgO)		•	•	•	•	•
Hematite (Fe_2O_3)	•	•	•	•	•	•
Anhydrite ($CaSO_4$)	•	•	•	•		
Arcanite (K_2SO_4)			•			
Cristobalite (SiO_2)					•	•
Wollastonite ($CaSiO_3$)					•	
Diopside ($CaMgSi_2O_6$)					•	•
Anorthite ($CaAl_2Si_2O_8$)				•	•	•
Leucite ($KAlSi_2O_6$)					•	•
Kalsilite ($KAlSiO_4$)	•	•	•	•		
Mullite ($Al_{2.35}Si_{0.64}O_{4.82}$)					•	•